

Preparation and characterization of new low melting ammonium-based ionic liquids with ether functionality

Minna Kärnä, Manu Lahtinen *, Jussi Valkonen

Department of Chemistry, University of Jyväskylä, P.O. Box 35, FI-40014 Jyväskylä, Finland

ARTICLE INFO

Article history:

Received 3 November 2008

Received in revised form 19 January 2009

Accepted 20 January 2009

Available online 31 January 2009

Keywords:

Quaternary ammonium bromide

Tetrafluoroborate

Hexafluorophosphate

Ionic liquid

Thermal analysis

X-ray diffraction

ABSTRACT

Eighteen new and three previously known but insufficiently characterized $R\hat{R}_3N^+A^-$ and $R_2\hat{R}_2N^+A^-$ type ($R = 2$ -ethoxyethyl or 4-methoxybenzyl, $\hat{R} =$ methyl, ethyl, *n*-propyl, *n*-butyl, *n*-pentyl or *n*-hexyl, $A =$ Br, BF_4 or PF_6) quaternary ammonium (QA) salts were synthesized and characterized by using 1H and ^{13}C NMR techniques, mass spectroscopy and elemental analysis. The bromide salts were synthesized either by treating dimethyl formamide with an ether functionalized alkyl bromide in the presence of potassium carbonate or by treating a tertiary amine with an ether functionalized alkyl bromide. The QA tetrafluoroborates and hexafluorophosphates were synthesized by metathesis reaction between a prepared QA bromide and HBF_4 or KPF_6 . The crystal structures of four compounds were determined by X-ray single crystal diffraction and powder diffraction was used to study the crystallinity of the solid compounds and to compare the structural similarities between the single crystals and the microcrystalline bulk form. Thermal properties of all compounds were studied by using TG/DTA and DSC methods. The anion exchange had a clear lowering effect on the melting points and enhanced the thermal stability of the BF_4^- and PF_6^- salts compared to the analogous bromides. Most of the compounds melted clearly below 100 °C, of which four are liquid at room temperature.

© 2009 Elsevier B.V. All rights reserved.

1. Introduction

The seemingly ever growing interest on room temperature ionic liquids (RTILs) has turned the spotlight, along with many others, to quaternary ammonium-based compounds. Ionic liquids are of interest because of their unique characteristics, for example, low vapor pressure and extraordinary solvent properties, which have enabled their use in numerous applications and which have been widely discussed in several excellent publications or reviews and references therein [1–6].

Traditionally, the most widespread applications of ionic liquids lie in organic synthesis as solvents and catalysts [7,8]. Ionic liquids have in fact been described as designer solvents since their properties can be tuned by careful selection of ionic species [1,9]. They have also various electrochemical applications: in electric double layer capacitors (energy storage device) ionic liquids have been used as electrolytes due to their high conductivity and some quaternary ammonium-based ionic liquids have been reported to have more potential than the traditional aromatic type ionic liquids such as imidazolium or pyridinium due to their higher cathodic stability [10,11]. The quest for new energy sources has also led a great attention to dye-sensitized solar cells (DSSCs) in which ionic liquids could be used to replace the organic liquid electrolytes due

to their non-volatility, non-flammability and high ionic conductivity, among other characteristics [12]. In addition to the most studied imidazolium-based ionic liquids, quaternary ammonium polyiodides have been tested as electrolytes in DSSCs [13]. Another solar application is the use of ionic liquids as heat-transfer fluids in electric power plants using parabolic trough solar collector technology [14–16]. Lately, some studies have suggested that ionic liquids could be used as a new class of lubricants or as additives in conventional lubricants. Certain quaternary ammonium-based ionic liquids have proven to be even more efficient lubricants than conventional hydrocarbon oils in reciprocal sliding tests [17]. Some ionic liquids containing a large amount of nitrogen are highly energetic materials which may be used in industrial or military applications [18]. A large number of tested applications consider only imidazolium-based ionic liquids which unfortunately are still rather expensive especially for large scale industrial applications. Quaternary ammonium and phosphonium-based ionic liquids, on the other hand, can also be made from readily available lower cost materials and thereby will be more applicable to industrial use if synthesized with reasonable yields [19–22]. Furthermore, the saturated quaternary ammonium cations are generally more resistant against oxidation and reduction than 1,3-substituted imidazolium cations that have certain degree of electrochemical instability and have some usability limitations in organic reactions [23,24]. Introducing an oxygen-containing side chain has proven to reduce the toxicity of imidazolium-based ionic liquids [25,26] and it might

* Corresponding author. Tel.: +358 14 2602624; fax: +358 14 2602501.
E-mail address: manu.lahtinen@jyu.fi (M. Lahtinen).

lead to a change of solvent properties [27,28]. Various methods to synthesize quaternary ammonium compounds has been known for a long time and a significant amount of publications exists [29–32]. Recently, a new method was developed by our group [33] for preparing $R_2\dot{R}_2N^+X^-$ type quaternary ammonium halides.

Relatively few studies on quaternary ammonium-based compounds with ether functionality have been made so far, for example, by Pernak [34], Das [35] and Hayamizu [36] and the number of existing compounds still remains fairly small comparing to, e.g., imidazolium-based compounds, and actually almost all are based to that cation. The number of simple acyclic non-chiral compounds is even smaller.

The aim of our studies is to find new quaternary ammonium-based compounds that have ionic liquid nature-compounds with a broad liquid range, low viscosity, good electrochemical properties and low melting point combined with good thermal stability. This is achieved by synthesizing new quaternary ammonium-based cations, pairing them with various anions, and performing systematic structural and thermoanalytical evaluations of the novel materials. Furthermore, based on special characteristics of the compounds potential application areas for the materials will be sought out in further studies.

In this study, as a continuum to our previous ones, 18 new $R_2\dot{R}_2N^+A^-$ or $\dot{R}R_3N^+A^-$ type quaternary ammonium (QA) salts, in which A is bromide, tetrafluoroborate or hexafluorophosphate, R is an

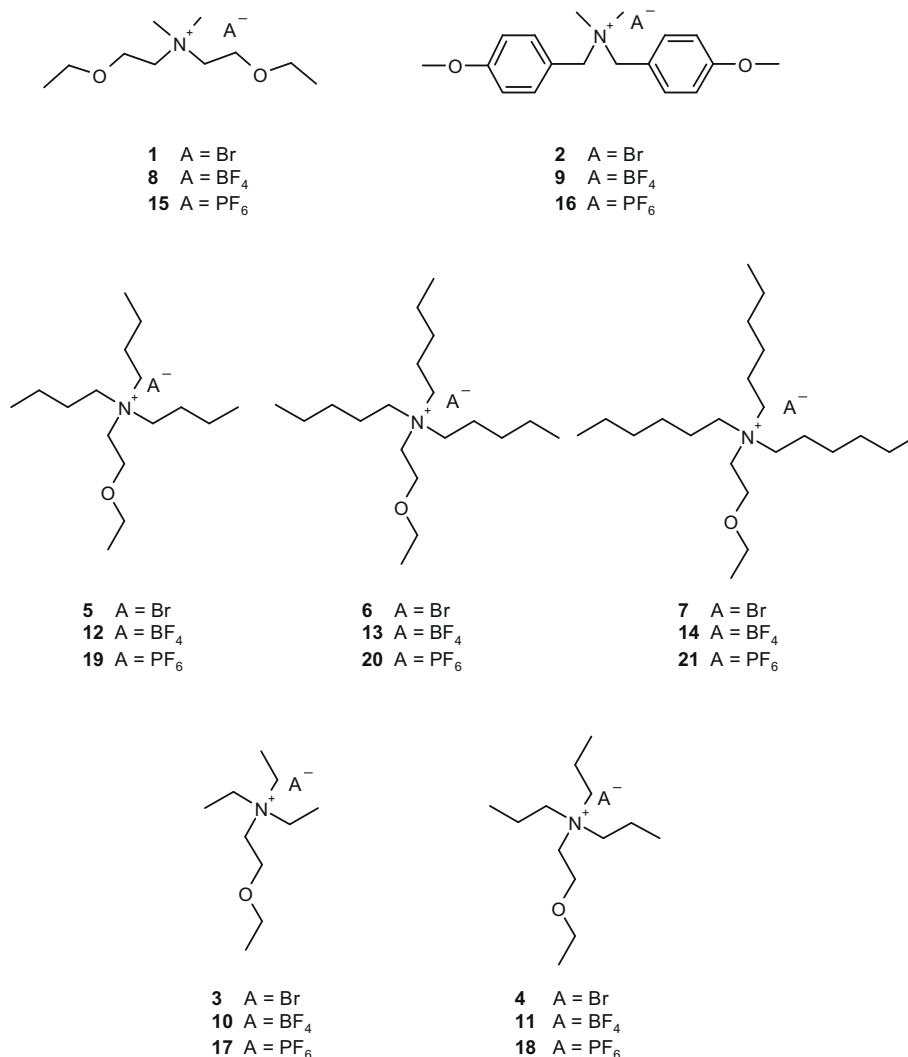
alkyl and R is an ether-bonded alkyl or aralkyl group, have been synthesized and characterized. In addition to these new compounds, three previously known but insufficiently characterized compounds [37–42] have been synthesized and characterized and used as precursors for six of the new QA salts. This study was oriented to structural characterization and thermal analysis and therefore the performed synthesis methods were not optimized. The 1H and ^{13}C NMR spectroscopy, elemental analysis and ESI-TOF MS measurements are used to verify the accuracy and the purity of the compounds. Furthermore, X-ray powder diffraction was used to study the crystallinity of the compounds and to compare the consistency between the single crystal structures and their powdery forms. The thermal properties have been observed by TG/DTA and DSC and the effect of different anions on some characteristics of the compounds have been examined by comparing these results.

2. Experimental

2.1. Synthesis and analysis

2.1.1. General procedure

All reagents and solvents were purchased from manufacturers and used as received. Compounds **1** and **2** (Scheme 1) were prepared by using the one-pot synthesis route described by Ropponen



Scheme 1. Molecular structure of the compounds 1–21.

et al. [33]. Reagents were placed in a reaction flask with an appropriate base and heated with continuous stirring at 65–70 °C for 96–168 h. Reaction mixture was cooled down to room temperature, filtered and filtrate containing the raw product was evaporated to a minimum volume. The final product was extracted by adding small amounts of diethyl ether or a mixture of diethyl ether and acetone which caused the precipitation of a white or light yellow powder. The products were recrystallized from dichloromethane and dried *in vacuo*.

Compounds **3–7** (Scheme 1) were synthesized applying the procedure explained by Albadran and McMurray [42]. Reagents and solvents were placed in a flask with a suitable solvent and refluxed at 70–76 °C for 24–168 h. After cooling to room temperature the mixtures were evaporated and the residues were washed with small amounts of a suitable solvent, i.e., diethyl ether and dried *in vacuo*.

Compounds **8–21** were synthesized by metathesis between one of the compounds **1–7** and a compound containing the desired anion. The tetrafluoroborates were synthesized by dissolving the QA bromide in a minimum volume of deionized water (further on, water) or other suitable solvent, i.e., acetone, and adding the stoichiometric amount (1:1) of 48–50 wt% solution of HBF₄. The mixture was stirred at room temperature for 2–30 min during which the QA tetrafluoroborate precipitated from the solution or formed a separate liquid layer. If other solvent than water was used, the product was obtained by evaporating the solvent. The raw product was filtered and washed with water until the washings were pH neutral. The product was recrystallized from an appropriate solvent, i.e., dichloromethane, and dried first in an incubator at 120 °C and then *in vacuo*. The liquid or waxy products were extracted with an appropriate solvent, i.e., dichloromethane, and dried as the solid products.

The hexafluorophosphates were synthesized by dissolving the QA bromide in a minimum volume of deionized water and adding the stoichiometric amount (1:1) of KPF₆ dissolved in a minimum amount of water. The mixture was stirred for 30 min at room temperature. The QA hexafluorophosphate precipitated from the solution or formed a separate liquid layer. The formed precipitate was filtered, washed with water and recrystallized from an appropriate solvent, i.e., dichloromethane and dried *in vacuo*. The liquid raw products were extracted with an appropriate solvent, evaporated and dried *in vacuo*.

2.1.2. Diethoxyethyl dimethylammonium bromide (1)

Reagents: 2-Bromoethylethyl ether (8.35 ml, 74.02 mmol), potassium carbonate (10.22 g, 74.02 mmol) and dimethyl formamide (50 ml). Reaction temperature 70 °C and reaction time 72 h. The yield (yellow sticky powder) was 2.76 g (28%). ¹H NMR (CDCl₃, 500 MHz, ppm): 1.13 (6H, t, –O–CH₂–CH₃), 3.41 (6H, s, N–CH₃), 3.49 (4H, q, –O–CH₂–CH₃), 3.85–3.86 (4H, m, N–CH₂–CH₂–O–), 3.89–3.90 (4H, m, N–CH₂–CH₂–O–). ¹³C NMR (CDCl₃, 126 MHz, ppm): 14.80 (2C, –O–CH₂–CH₃), 52.66 (2C, N–CH₃), 64.26 (2C, N–CH₂–CH₂–O), 64.74 (2C, N–CH₂–CH₂–O), 66.83 (2C, –O–CH₂–CH₃). ESI-TOF MS: *m/z* calculated for C₁₀H₂₄NBr [M–Br]⁺: 190.18; found 190.14 [M–Br]⁺. Elemental analysis: calculated for C₁₀H₂₄NBr: C, 44.45; H, 8.95; N, 5.18. Found C, 44.16; H, 8.78; N, 4.85.

2.1.3. Di-(4-methoxybenzyl) dimethylammonium bromide (2)

Reagents: 4-Methoxybenzyl bromide (5 g, 24.88 mmol), potassium carbonate (3.77 g, 27.28 mmol) and dimethyl formamide (25 ml). Reaction temperature 70 °C and reaction time 96 h. The yield (white powder) was 1.74 g (40%). ¹H NMR (CDCl₃, 500 MHz, ppm): 3.03 (6H, s, N–CH₃), 3.76 (6H, s, –O–CH₃), 5.03 (4H, s, N–CH₂–), 6.85 (4H, d, Ar–H), 7.56 (4H, d, Ar–H). ¹³C NMR (CDCl₃, 126 MHz, ppm): 47.64 (2C, N–CH₃), 55.38 (2C, –O–CH₃), 67.01 (2C, N–CH₂–), 114.48 (4C, Ar–C), 119.37 (1C, Ar–C), 134.78 (4C, Ar–C), 161.24 (1C, Ar–C). ESI-TOF MS: *m/z* calculated for

C₁₈H₂₄NO₂Br [M–Br]⁺: 286.18; found 286.14 [M–Br]⁺. Elemental analysis: calculated for C₁₈H₂₄NO₂Br: C, 59.02; H, 6.60; N, 3.82. Found C, 59.35; H, 6.65; N, 3.70.

2.1.4. Triethyl ethoxyethylammonium bromide (3)

Reagents: Triethylamine (10.99 ml, 79.10 mmol), 2-bromoethylethyl ether (7.40 ml, 66.00 mmol), methanol (25 ml). Reaction temperature 70 °C and reaction time 72 h. The yield (white powder) was 15.08 g (90%). ¹H NMR (CDCl₃, 500 MHz, ppm): 1.15 (3H, –O–CH₂–CH₃), 1.39 (9H, t, N–CH₂–CH₃), 3.49–3.57 (8H, N–CH₂–CH₃, –O–CH₂–CH₃), 3.72–3.74 (2H, m, N–CH₂–CH₂–O–), 3.84–3.85 (2H, m, N–CH₂–CH₂–O–). ¹³C NMR (CDCl₃, 126 MHz, ppm): 8.17 (3C, N–CH₂–CH₃), 14.85 (1C, –O–CH₂–CH₃), 54.33 (3C, N–CH₂–CH₃), 57.50 (1C, N–CH₂–CH₂–O–), 3.89 (1C, N–CH₂–CH₂–O–), 67.05 (1C, –O–CH₂–CH₃). ESI-TOF MS: *m/z* calculated for C₁₀H₂₄NOBr [M–Br]⁺: 174.19; found 174.18 [M–Br]⁺. Elemental analysis: calculated for C₁₀H₂₄NOBr: C, 47.25; H, 9.52; N, 5.51. Found C, 46.37; H, 9.52; N, 5.57.

2.1.5. Tripropyl ethoxyethylammonium bromide (4)

Reagents: Tripropylamine (15.05 ml, 79.10 mmol), 2-bromoethylethyl ether (7.40 ml, 66.00 mmol), methanol (25 ml). Reaction temperature 70 °C and reaction time 72 h. The yield (white powder) was 11.54 g (59%). ¹H NMR (CDCl₃, 500 MHz, ppm): 1.00 (9H, t, N–CH₂–CH₂–CH₃), 1.15 (3H, t, –O–CH₂–CH₃), 1.73–1.79 (6H, m, N–CH₂–CH₂–CH₃), 3.33–3.37 (6H, m, N–CH₂–CH₂–CH₃), 3.50 (2H, q, –O–CH₂–CH₃), 3.86 (4H, m, N–(CH₂)₂–O–). ¹³C NMR (CDCl₃, 126 MHz, ppm): 10.73 (3C, N–CH₂–CH₂–CH₃), 14.94 (1C, –O–CH₂–CH₃), 15.95 (3C, N–CH₂–CH₂–CH₃), 59.21 (1C, N–CH₂–CH₂–O), 61.44 (3C, N–CH₂–CH₂–CH₃), 64.12 (1C, N–CH₂–CH₂–O), 67.06 (1C, –O–CH₂–CH₃). ESI-TOF MS: *m/z* calculated for C₁₃H₃₀NOBr [M–Br]⁺: 216.18; found 216.23 [M–Br]⁺. Elemental analysis: calculated for C₁₃H₃₀NOBr: C, 52.70; H, 10.21; N, 4.73. Found C, 52.45; H, 9.84; N, 4.68.

2.1.6. Tributyl ethoxyethylammonium bromide (5)

Reagents: Tributylamine (18.84 ml, 79.10 mmol), 2-bromoethylethyl ether (7.40 ml, 66.00 mmol), methanol (25 ml). Reaction temperature 70 °C and reaction time 144 h. The yield (white powder) was 15.73 g (71%). ¹H NMR (CDCl₃, 500 MHz, ppm): 0.98 (9H, t, N–CH₂–CH₂–CH₂–CH₃), 1.15 (3H, t, –O–CH₂–CH₃), 1.37–1.43 (6H, m, N–CH₂–CH₂–CH₂–CH₃), 1.66–1.72 (6H, m, N–CH₂–CH₂–CH₂–CH₃), 3.36–3.39 (6H, m, N–CH₂–CH₂–CH₂–CH₃), 3.50 (2H, q, –O–CH₂–CH₃), 3.86 (4H, m, N–(CH₂)₂–O–). ¹³C NMR (CDCl₃, 126 MHz, ppm): 13.55 (3C, N–CH₂–CH₂–CH₂–CH₃), 14.91 (1C, –O–CH₂–CH₃), 19.68 (3C, N–CH₂–CH₂–CH₂–CH₃), 24.17 (3C, N–CH₂–CH₂–CH₂–CH₃), 59.24 (1C, N–CH₂–CH₂–O), 59.82 (3C, N–CH₂–CH₂–CH₂–CH₃), 64.19 (1C, N–CH₂–CH₂–O), 67.08 (1C, –O–CH₂–CH₃). ESI-TOF MS: *m/z* calculated for C₁₆H₃₆NOBr [M–Br]⁺: 258.30; found 258.30 [M–Br]⁺. Elemental analysis: calculated for C₁₆H₃₆NOBr: C, 56.79; H, 10.72; N, 4.14. Found C, 56.50; H, 10.85; N, 4.16.

2.1.7. Tripentyl ethoxyethylammonium bromide (6)

Reagents: Tripentylamine (22.80 ml, 79.10 mmol), 2-bromoethylethyl ether (7.40 ml, 66.00 mmol), methanol (25 ml). Reaction temperature 70 °C and reaction time 144 h. The yield (yellow sticky powder) was 8.05 g (32%). ¹H NMR (CDCl₃, 500 MHz, ppm): 0.91 (9H, t, N–CH₂–CH₂–CH₂–CH₂–CH₃), 1.17 (3H, t, –O–CH₂–CH₃), 1.32–1.41 (12H, m, N–CH₂–CH₂–(CH₂)₂–CH₃), 1.68–1.75 (6H, m, N–CH₂–CH₂–CH₂–CH₂–CH₃), 3.35–3.39 (6H, m, N–CH₂–CH₂–CH₂–CH₂–CH₃), 3.52 (2H, q, –O–CH₂–CH₃), 3.89 (2H, m, N–CH₂–CH₂–O–), 3.91–3.93 (2H, m, N–CH₂–CH₂–O–). ¹³C NMR (CDCl₃, 126 MHz, ppm): 13.77 (3C, N–CH₂–CH₂–CH₂–CH₂–CH₃), 14.97 (1C, –O–CH₂–CH₃), 22.02 (3C, N–CH₂–CH₂–CH₂–CH₂–CH₃), 22.15 (3C, N–CH₂–CH₂–CH₂–CH₂–CH₃), 28.42 (3C, N–CH₂–CH₂–

CH₂–CH₂–CH₃), 59.37 (1C, N–CH₂–CH₂–O–), 60.04 (1C, N–CH₂–CH₂–CH₂–CH₂–CH₃), 64.27 (1C, N–CH₂–CH₂–O–), 67.13 (1C, –O–CH₂–CH₃). ESI-TOF MS: *m/z* calculated for C₁₉H₄₂NOBr [M–Br]⁺: 300.29; found 300.33 [M–Br]⁺. Elemental analysis: calculated for C₁₉H₄₂NOBr: C, 59.98; H, 11.13; N, 3.68. Found C, 59.73; H, 11.28; N, 3.36.

2.1.8. Trihexyl ethoxyethylammonium bromide (7)

Reagents: Trihexylamine (26.70 ml, 79.10 mmol), 2-bromoethyl ether (7.40 ml, 66.00 mmol), methanol (25 ml). Reaction temperature 70 °C and reaction time 168 h. The yield (white powder) was 11.47 g (41%). ¹H NMR (CDCl₃, 500 MHz, ppm): 0.88 (9H, t, N–CH₂–CH₂–CH₂–CH₂–CH₂–CH₃), 1.16 (3H, t, –O–CH₂–CH₃), 1.28–1.37 (18H, m, N–CH₂–CH₂–(CH₂)₃–CH₃), 1.66–1.73 (6H, m, N–CH₂–CH₂–CH₂–CH₂–CH₂–CH₃), 3.34–3.37 (6H, m, N–CH₂–CH₂–CH₂–CH₂–CH₂–CH₃), 3.51 (2H, q, O–CH₂–CH₃), 3.87–3.90 (4H, m, N–CH₂–CH₂–O–). ¹³C NMR (CDCl₃, 126 MHz, ppm): 13.77 (3C, N–CH₂–CH₂–CH₂–CH₂–CH₂–CH₃), 14.95 (1C, –O–CH₂–CH₃), 22.26 (3C, N–CH₂–CH₂–CH₂–CH₂–CH₂–CH₃), 22.35 (3C, N–CH₂–CH₂–CH₂–CH₂–CH₂–CH₃), 26.01 (3C, N–CH₂–CH₂–CH₂–CH₂–CH₂–CH₃), 31.20 (3C, N–CH₂–CH₂–CH₂–CH₂–CH₂–CH₃), 59.31 (1C, N–CH₂–CH₂–O), 60.00 (3C, N–CH₂–CH₂–CH₂–CH₂–CH₂–CH₃), 64.25 (1C, N–CH₂–CH₂–O), 67.10 (1C, O–CH₂–CH₃). ESI-TOF MS: *m/z* calculated for C₂₂H₄₈NOBr [M–Br]⁺: 342.37; found 342.37 [M–Br]⁺. Elemental analysis: calculated for C₂₂H₄₈NOBr: C, 62.54; H, 11.45; N, 3.31. Found C, 63.03; H, 11.45; N, 3.31.

2.1.9. Diethoxyethyl dimethylammonium tetrafluoroborate (8)

Reagents: Diethoxyethyl dimethylammonium bromide (1) (1.0 g, 3.7 mmol) and HBF₄ solution (48–50 wt%). The yield (brown gel) was 1.0 g (97%). ¹H NMR (CDCl₃, 500 MHz, ppm): 1.19 (6H, t, –O–CH₂–CH₃), 3.23 (6H, s, N–CH₃), 3.53 (4H, q, –O–CH₂–CH₃), 3.62–3.66 (4H, m, N–CH₂–CH₂–O–), 3.84–3.86 (4H, m, N–CH₂–CH₂–O–). ¹³C NMR (CDCl₃, 126 MHz, ppm): 14.85 (2C, –O–CH₂–CH₃), 52.48 (2C, N–CH₃), 64.06 (2C, N–CH₂–CH₂–O), 64.96 (2C, N–CH₂–CH₂–O), 66.89 (2C, –O–CH₂–CH₃). ESI-TOF MS: *m/z* calculated for C₁₀H₂₄NBF₄ [M–BF₄]⁺: 190.18; found 190.14 [M–BF₄]⁺. Elemental analysis: calculated for C₁₀H₂₄NBF₄: C, 43.34; H, 8.73; N, 5.05. Found C, 41.13; H, 8.18; N, 5.15.

2.1.10. Di-(4-methoxybenzyl) dimethylammonium tetrafluoroborate (9)

Reagents: Di-(4-methoxybenzyl) dimethylammonium bromide (2) (1.0 g, 2.7 mmol) and HBF₄ solution (48–50 wt%). The yield (white powder) was 0.9 g (88%). ¹H NMR (CDCl₃, 500 MHz, ppm): 2.85 (6H, s, N–CH₃), 3.79 (6H, s, –O–CH₃), 4.58 (4H, s, N–CH₂–), 6.89 (4H, d, Ar–H), 7.44 (4H, d, Ar–H). ¹³C NMR (CDCl₃, 126 MHz, ppm): 47.41 (2C, N–CH₃), 55.35 (2C, –O–CH₃), 67.94 (2C, N–CH₂–), 114.62 (4C, Ar–C), 118.86 (2C, Ar–C), 134.57 (4C, Ar–C), 161.38 (2C, Ar–C). ESI-TOF MS: *m/z* calculated for C₁₈H₂₄NO₂BF₄ [M–BF₄]⁺: 286.18; found 286.11 [M–BF₄]⁺. Elemental analysis: calculated for C₁₈H₂₄NO₂BF₄: C, 57.93; H, 6.48; N, 3.75. Found C, 58.12; H, 6.57; N, 3.44.

2.1.11. Triethyl ethoxyethylammonium tetrafluoroborate (10)

Reagents: Triethyl ethoxyethylammonium bromide (3) (1.0 g, 4.3 mmol) and HBF₄ solution (48–50 wt%). The yield (clear colorless gel) was 0.9 g (79%). ¹H NMR (CDCl₃, 500 MHz, ppm): 1.18 (3H, t, –O–CH₂–CH₃), 1.34 (9H, t, N–CH₂–CH₃), 3.41 (6H, q, N–CH₂–CH₃), 3.47 (2H, m, N–CH₂–CH₂–O–), 3.52 (2H, q, –O–CH₂–CH₃), 3.80 (2H, m, N–CH₂–CH₂–O–). ¹³C NMR (CDCl₃, 126 MHz, ppm): 7.57 (3C, N–CH₂–CH₃), 14.86 (1C, –O–CH₂–CH₃), 53.96 (3C, N–CH₂–CH₃), 56.91 (1C, N–CH₂–CH₂–O–), 63.59 (1C, N–CH₂–CH₂–O–), 67.07 (1C, –O–CH₂–CH₃). ESI-TOF MS: *m/z* calculated for C₁₀H₂₄NOBF₄ [M–BF₄]⁺: 174.13; found 174.13 [M–BF₄]⁺. Elemental analysis: calculated for C₁₀H₂₄NOBF₄: C, 46.00; H, 9.26; N, 5.36. Found C, 45.63; H, 10.13; N, 5.72.

2.1.12. Tripropyl ethoxyethylammonium tetrafluoroborate (11)

Reagents: Tripropyl ethoxyethylammonium bromide (4) (1.0 g, 3.4 mmol) and HBF₄ solution (48–50 wt%). The yield (yellow wax) was 0.8 g (82%). ¹H NMR (CDCl₃, 500 MHz, ppm): 0.99 (9H, t, N–CH₂–CH₂–CH₃), 1.17 (3H, t, –O–CH₂–CH₃), 1.67–1.75 (6H, m, N–CH₂–CH₂–CH₃), 3.21–3.24 (6H, m, N–CH₂–CH₂–CH₃), 3.50 (2H, q, –O–CH₂–CH₃), 3.52 (2H, m, N–CH₂–CH₂–O–), 3.78 (2H, m, N–CH₂–CH₂–O–), 14.91 (1C, –O–CH₂–CH₃), 15.49 (3C, N–CH₂–CH₂–CH₃), 58.48 (1C, N–CH₂–CH₂–O), 61.12 (3C, N–CH₂–CH₂–CH₃), 63.71 (1C, N–CH₂–CH₂–O), 66.99 (1C, –O–CH₂–CH₃). ESI-TOF MS: *m/z* calculated for C₁₃H₃₀NOBF₄ [M–BF₄]⁺: 216.23; found 216.20 [M–BF₄]⁺. Elemental analysis: calculated for C₁₃H₃₀NOBF₄: C, 51.50; H, 9.97; N, 4.62. Found C, 50.41; H, 10.13; N, 4.66.

2.1.13. Tributyl ethoxyethylammonium tetrafluoroborate (12)

Reagents: Tributyl ethoxyethylammonium bromide (5) (1.0 g, 3.0 mmol) and HBF₄ solution (48–50 wt%). The yield (white powder) was 0.5 g (54%). ¹H NMR (CDCl₃, 500 MHz, ppm): 0.99 (9H, t, N–CH₂–CH₂–CH₂–CH₃), 1.17 (3H, t, –O–CH₂–CH₃), 1.36–1.42 (6H, m, N–CH₂–CH₂–CH₂–CH₃), 1.61–1.68 (6H, m, N–CH₂–CH₂–CH₂–CH₃), 3.24–3.28 (6H, m, N–CH₂–CH₂–CH₂–CH₃), 3.50 (2H, q, –O–CH₂–CH₃), 3.53–3.55 (2H, m, N–CH₂–CH₂–O–), 3.78 (2H, m, N–CH₂–CH₂–O–). ¹³C NMR (CDCl₃, 126 MHz, ppm): 13.49 (3C, N–CH₂–CH₂–CH₂–CH₃), 14.90 (1C, –O–CH₂–CH₃), 19.59 (3C, N–CH₂–CH₂–CH₂–CH₃), 22.81 (3C, N–CH₂–CH₂–CH₂–CH₃), 58.43 (1C, N–CH₂–CH₂–O), 59.48 (3C, N–CH₂–CH₂–CH₂–CH₃), 63.80 (1C, N–CH₂–CH₂–O), 67.05 (1C, –O–CH₂–CH₃). ESI-TOF MS: *m/z* calculated for C₁₃H₃₀NOBF₄ [M–BF₄]⁺: 258.28; found 258.26 [M–BF₄]⁺. Elemental analysis: calculated for C₁₃H₃₀NOBF₄: C, 55.66; H, 10.51; N, 4.06. Found C, 55.30; H, 10.49; N, 3.66.

2.1.14. Tripentyl ethoxyethylammonium tetrafluoroborate (13)

Reagents: Tripentyl ethoxyethylammonium bromide (6) (1.0 g, 2.6 mmol) and HBF₄ solution (48–50 wt%). The yield (yellow sticky powder) was 0.8 g (75%). ¹H NMR (CDCl₃, 500 MHz, ppm): 0.91 (9H, t, N–CH₂–CH₂–CH₂–CH₂–CH₃), 1.17 (3H, t, –O–CH₂–CH₃), 1.33–1.40 (12H, m, N–CH₂–CH₂–(CH₂)₂–CH₃), 1.62–1.70 (6H, m, N–CH₂–CH₂–CH₂–CH₂–CH₃), 3.23–3.26 (6H, m, N–CH₂–CH₂–CH₂–CH₂–CH₃), 3.50 (2H, q, –O–CH₂–CH₃), 3.54–3.55 (2H, m, N–CH₂–CH₂–O–), 3.76–3.77 (2H, m, N–CH₂–CH₂–O–). ¹³C NMR (CDCl₃, 126 MHz, ppm): 13.72 (3C, N–CH₂–CH₂–CH₂–CH₂–CH₃), 14.91 (1C, –O–CH₂–CH₃), 21.57 (3C, N–CH₂–CH₂–CH₂–CH₂–CH₃), 23.18 (3C, N–CH₂–CH₂–CH₂–CH₂–CH₃), 28.25 (3C, N–CH₂–CH₂–CH₂–CH₂–CH₃), 58.39 (1C, N–CH₂–CH₂–O), 59.61 (1C, N–CH₂–CH₂–CH₂–CH₂–CH₃), 63.80 (1C, N–CH₂–CH₂–O), 67.04 (1C, –O–CH₂–CH₃). ESI-TOF MS: *m/z* calculated for C₁₉H₄₂NOBF₄ [M–BF₄]⁺: 300.33; found 300.26 [M–BF₄]⁺. Elemental analysis: calculated for C₁₉H₄₂NOBF₄: C, 58.93; H, 10.93; N, 3.62. Found C, 58.66; H, 11.06; N, 3.59.

2.1.15. Trihexyl ethoxyethylammonium tetrafluoroborate (14)

Reagents: Trihexyl ethoxyethylammonium bromide (7) (1.0 g, 2.4 mmol) and HBF₄ solution (48–50 wt%). The yield (yellow sticky powder) was 0.9 g (85%). ¹H NMR (CDCl₃, 500 MHz, ppm): 0.90 (9H, t, N–CH₂–CH₂–CH₂–CH₂–CH₂–CH₃), 1.18 (3H, t, –O–CH₂–CH₃), 1.29–1.37 (18H, m, N–CH₂–CH₂–(CH₂)₃–CH₃), 1.63–1.67 (6H, m, N–CH₂–CH₂–CH₂–CH₂–CH₂–CH₃), 3.23–3.26 (6H, m, N–CH₂–CH₂–CH₂–CH₂–CH₂–CH₃), 3.51 (2H, q, O–CH₂–CH₃), 3.56–3.58 (2H, m, N–CH₂–CH₂–O–), 3.78–3.79 (2H, m, N–CH₂–CH₂–O–). ¹³C NMR (CDCl₃, 126 MHz, ppm): 13.79 (3C, N–CH₂–CH₂–CH₂–CH₂–CH₂–CH₃), 14.93 (1C, –O–CH₂–CH₃), 21.88 (3C, N–CH₂–CH₂–CH₂–CH₂–CH₂–CH₃), 22.34 (3C, N–CH₂–CH₂–CH₂–CH₂–CH₂–CH₃), 25.89 (3C, N–CH₂–CH₂–CH₂–CH₂–CH₂–CH₃), 31.09 (3C, N–CH₂–CH₂–CH₂–CH₂–CH₂–CH₃), 58.48 (1C, N–CH₂–CH₂–O), 59.67 (3C, N–CH₂–CH₂–CH₂–CH₂–CH₂–CH₃), 63.85 (1C, N–CH₂–CH₂–O), 67.09 (1C,

O-CH₂-CH₃). ESI-TOF MS: *m/z* calculated for C₂₂H₄₈NOBF₄ [M-BF₄]⁺: 342.37; found 342.35 [M-BF₄]⁺. Elemental analysis: calculated for C₂₂H₄₈NOBF₄: C, 61.53; H, 11.27; N, 3.26. Found C, 61.41; H, 11.27; N, 2.96.

2.1.16. Diethoxyethyltrimethylammonium hexafluorophosphate (15)

Reagents: Diethoxyethyltrimethylammonium bromide (1) (1.0 g, 3.7 mmol) and KPF₆ (0.68 g, 3.7 mmol). The yield (yellow gel) was 0.8 g (64%). ¹H NMR (CDCl₃, 500 MHz, ppm): 1.1 (6H, t, -O-CH₂-CH₃), 3.19 (6H, s, N-CH₃), 3.52 (4H, q, -O-CH₂-CH₃), 3.57–3.59 (4H, m, N-CH₂-CH₂-O-), 3.81–3.83 (4H, m, N-CH₂-CH₂-O-). ¹³C NMR (CDCl₃, 126 MHz, ppm): 14.79 (2C, -O-CH₂-CH₃), 52.51 (2C, N-CH₃), 63.91 (2C, N-CH₂-CH₂-O), 65.01 (2C, N-CH₂-CH₂-O), 66.87 (2C, -O-CH₂-CH₃). ESI-TOF MS: *m/z* calculated for C₁₀H₂₄NO₂PF₆ [M-PF₆]⁺: 190.18; found 190.17 [M-PF₆]⁺. Elemental analysis: calculated for C₁₀H₂₄NO₂PF₆: C, 35.82; H, 7.22; N, 4.18. Found C, 35.85; H, 7.04; N, 4.04.

2.1.17. Di-(4-methoxybenzyl)dimethylammonium hexafluorophosphate (16)

Reagents: Di-(4-methoxybenzyl)dimethylammonium bromide (2) (1.0 g, 2.7 mmol) and KPF₆ (0.50 g, 2.7 mmol). The yield (white crystals) was 0.7 g (63%). ¹H NMR (DMSO, 500 MHz, ppm): 2.78 (6H, s, N-CH₃), 3.81 (6H, s, -O-CH₃), 4.47 (4H, s, N-CH₂-), 7.06 (4H, d, Ar-H), 7.49 (4H, d, Ar-H). ¹³C NMR (DMSO, 126 MHz, ppm): 47.57 (2C, N-CH₃), 55.23 (2C, -O-CH₃), 66.67 (2C, N-CH₂-), 114.28 (4C, Ar-C), 119.67 (1C, Ar-C), 134.44 (4C, Ar-C), 160.60 (1C, Ar-C). ESI-TOF MS: *m/z* calculated for C₁₈H₂₄NO₂PF₆ [M-PF₆]⁺: 286.13; found 286.13 [M-PF₆]⁺. Elemental analysis: calculated for C₁₈H₂₄NO₂PF₆: C, 50.12; H, 5.61; N, 3.25. Found C, 50.43; H, 5.65; N, 2.74.

2.1.18. Triethyl ethoxyethylammonium hexafluorophosphate (17)

Reagents: Triethyl ethoxyethylammonium bromide (3) (1.0 g, 4.3 mmol) and KPF₆ (0.80 g, 4.3 mmol). The yield (yellow gel) was 1.1 g (81%). ¹H NMR (CDCl₃, 500 MHz, ppm): 1.18 (3H, t, -O-CH₂-CH₃), 1.34 (9H, t, N-CH₂-CH₃), 3.36 (6H, q, N-CH₂-CH₃), 3.40–3.42 (2H, m, N-CH₂-CH₂-O-), 3.52 (2H, q, -O-CH₂-CH₃), 3.77 (2H, m, N-CH₂-CH₂-O-). ¹³C NMR (CDCl₃, 126 MHz, ppm): 7.44 (3C, N-CH₂-CH₃), 14.81 (1C, -O-CH₂-CH₃), 53.97 (3C, N-CH₂-CH₃), 56.87 (1C, N-CH₂-CH₂-O-), 63.44 (1C, N-CH₂-CH₂-O-), 67.09 (1C, -O-CH₂-CH₃). ESI-TOF MS: *m/z* calculated for C₁₀H₂₄NO₂PF₆ [M-PF₆]⁺: 174.19; found 174.15 [M-PF₆]⁺. Elemental analysis: calculated for C₁₀H₂₄NO₂PF₆: C, 37.62; H, 7.58; N, 4.39. Found C, 37.39; H, 7.37; N, 4.42.

2.1.19. Tripropyl ethoxyethylammonium hexafluorophosphate (18)

Reagents: Tripropyl ethoxyethylammonium bromide (4) (1.0 g, 3.4 mmol) and KPF₆ (0.62 g, 3.4 mmol). The yield (white powder) was 0.9 g (77%). ¹H NMR (CDCl₃, 500 MHz, ppm): 0.99 (9H, t, N-CH₂-CH₂-CH₃), 1.18 (3H, t, -O-CH₂-CH₃), 1.66–1.74 (6H, m, N-CH₂-CH₂-CH₃), 3.18–3.21 (6H, m, N-CH₂-CH₂-CH₃), 3.46–3.47 (2H, m, N-CH₂-CH₂-O-), 3.50 (2H, q, -O-CH₂-CH₃), 3.76 (2H, m, N-CH₂-CH₂-O-). ¹³C NMR (CDCl₃, 126 MHz, ppm): 10.42 (3C, N-CH₂-CH₂-CH₃), 14.88 (1C, -O-CH₂-CH₃), 15.43 (3C, N-CH₂-CH₂-CH₃), 58.47 (1C, N-CH₂-CH₂-O), 61.14 (3C, N-CH₂-CH₂-CH₃), 63.56 (1C, N-CH₂-CH₂-O), 67.04 (1C, -O-CH₂-CH₃). ESI-TOF MS: *m/z* calculated for C₁₃H₃₀NO₂PF₆ [M-PF₆]⁺: 216.23; found 216.22 [M-PF₆]⁺. Elemental analysis: calculated for C₁₃H₃₀NO₂PF₆: C, 43.21; H, 8.37; N, 3.88. Found C, 43.25; H, 8.67; N, 3.92.

2.1.20. Tributyl ethoxyethylammonium hexafluorophosphate (19)

Reagents: Tributyl ethoxyethylammonium bromide (5) (1.0 g, 3.0 mmol) and KPF₆ (0.54 g, 3.0 mmol). The yield (white powder) was 1.0 g (77%). ¹H NMR (CDCl₃, 500 MHz, ppm): 0.99 (9H, t, N-CH₂-CH₂-CH₂-CH₃), 1.18 (3H, t, -O-CH₂-CH₃), 1.38–1.42 (6H, m,

N-CH₂-CH₂-CH₂-CH₃), 1.60–1.66 (6H, m, N-CH₂-CH₂-CH₂-CH₃), 3.31–3.25 (6H, m, N-CH₂-CH₂-CH₂-CH₃), 3.48–3.53 (4H, m, N-CH₂-CH₂-O-CH₂-CH₃), 3.76–3.77 (2H, m, N-CH₂-CH₂-O-). ¹³C NMR (CDCl₃, 126 MHz, ppm): 13.45 (3C, N-CH₂-CH₂-CH₂-CH₃), 14.87 (1C, -O-CH₂-CH₃), 19.55 (3C, N-CH₂-CH₂-CH₂-CH₃), 23.78 (3C, N-CH₂-CH₂-CH₂-CH₃), 58.42 (1C, N-CH₂-CH₂-O), 59.52 (3C, N-CH₂-CH₂-CH₂-CH₃), 63.68 (1C, N-CH₂-CH₂-O-), 67.14 (1C, -O-CH₂-CH₃). ESI-TOF MS: *m/z* calculated for C₁₆H₃₆NO₂PF₆ [M-PF₆]⁺: 258.28; found 258.26 [M-PF₆]⁺. Elemental analysis: calculated for C₁₆H₃₆NO₂PF₆: C, 47.63; H, 8.99; N, 3.47. Found C, 47.93; H, 9.20; N, 3.48.

2.1.21. Tripentyl ethoxyethylammonium hexafluorophosphate (20)

Reagents: Tripentyl ethoxyethylammonium bromide (6) (1.0 g, 2.6 mmol) and KPF₆ (0.48 g, 2.6 mmol). The yield (white powder) was 1.0 g (85%). ¹H NMR (CDCl₃, 500 MHz, ppm): 0.92 (9H, t, N-CH₂-CH₂-CH₂-CH₂-CH₃), 1.18 (3H, t, O-CH₂-CH₃), 1.31–1.41 (12H, m, N-CH₂-CH₂-(CH₂)₂-CH₃), 1.61–1.67 (6H, m, N-CH₂-CH₂-CH₂-CH₂-CH₃), 3.20–3.24 (6H, m, N-CH₂-CH₂-CH₂-CH₂-CH₃), 3.48–3.53 (4H, m, N-CH₂-CH₂-O-CH₂-CH₃), 3.75–3.76 (2H, m, N-CH₂-CH₂-O-). ¹³C NMR (CDCl₃, 126 MHz, ppm): 13.71 (3C, N-CH₂-CH₂-CH₂-CH₂-CH₃), 14.89 (1C, O-CH₂-CH₃), 21.55 (3C, N-CH₂-CH₂-CH₂-CH₂-CH₃), 22.07 (3C, N-CH₂-CH₂-CH₂-CH₂-CH₃), 28.20 (3C, N-CH₂-CH₂-CH₂-CH₂-CH₃), 58.38 (1C, N-CH₂-CH₂-O-), 59.66 (3C, N-CH₂-CH₂-CH₂-CH₂-CH₃), 63.69 (1C, N-CH₂-CH₂-O-), 67.14 (1C, O-CH₂-CH₃). ESI-TOF MS: *m/z* calculated for C₁₉H₄₂NO₂PF₆ [M-PF₆]⁺: 300.32; found 300.32 [M-PF₆]⁺. Elemental analysis: calculated for C₁₉H₄₂NO₂PF₆: C, 51.22; H, 9.50; N, 3.14. Found C, 51.60; H, 9.78; N, 3.18.

2.1.22. Trihexyl ethoxyethylammonium hexafluorophosphate (21)

Reagents: Trihexyl ethoxyethylammonium bromide (7) (1.0 g, 2.4 mmol) and KPF₆ (0.44 g, 2.4 mmol). The yield (white powder) was 1.0 g (89%). ¹H NMR (CDCl₃, 500 MHz, ppm): 0.89 (9H, t, N-CH₂-CH₂-CH₂-CH₂-CH₂-CH₃), 1.18 (3H, t, O-CH₂-CH₃), 1.32–1.37 (18H, m, N-CH₂-CH₂-(CH₂)₃-CH₃), 1.60–1.65 (6H, m, N-CH₂-CH₂-CH₂-CH₂-CH₂-CH₃), 3.20–3.23 (6H, m, N-CH₂-CH₂-CH₂-CH₂-CH₂-CH₃), 3.48–3.53 (4H, m, N-CH₂-CH₂-O-CH₂-CH₃), 3.75–3.76 (2H, m, N-CH₂-CH₂-O-CH₂-CH₃). ¹³C NMR (CDCl₃, 126 MHz, ppm): 13.77 (3C, N-CH₂-CH₂-CH₂-CH₂-CH₂-CH₃), 14.90 (1C, O-CH₂-CH₃), 21.82 (3C, N-CH₂-CH₂-CH₂-CH₂-CH₂-CH₃), 22.33 (3C, N-CH₂-CH₂-CH₂-CH₂-CH₂-CH₃), 25.81 (3C, N-CH₂-CH₂-CH₂-CH₂-CH₂-CH₃), 31.04 (3C, N-CH₂-CH₂-CH₂-CH₂-CH₂-CH₃), 58.39 (1C, N-CH₂-CH₂-O-), 59.68 (3C, N-CH₂-CH₂-CH₂-CH₂-CH₂-CH₃), 63.70 (1C, N-CH₂-CH₂-O-), 67.15 (1C, O-CH₂-CH₃). ESI-TOF MS: *m/z* calculated for C₂₂H₄₈NO₂PF₆ [M-PF₆]⁺: 342.37; found 342.32 [M-PF₆]⁺. Elemental analysis: calculated for C₂₂H₄₈NO₂PF₆: C, 54.19; H, 9.92; N, 2.87. Found C, 54.47; H, 10.01; N, 2.50.

2.2. Characterization in the liquid state

The formation of the desired products was confirmed by ¹H and ¹³C NMR spectroscopy and ESI-TOF mass spectroscopy. Elemental analysis was used to verify the purity of the formed compounds. ¹H and ¹³C NMR spectra were measured in CDCl₃ (or appropriate solvent) at 30 °C by using a Bruker Avance DRX 500 NMR spectrometer operating at 500 MHz for ¹H and at 126 MHz for ¹³C. Mass spectra were obtained by using the Micromass LCT time of flight (TOF) mass spectrometer with electrospray ionization (ESI). The measurements were made by using the positive ion mode with a sample concentration of 25 mg/l in a methanol solution. When necessary, the absence of the bromide-ion was confirmed by using the negative ion mode. The elemental analyses were carried out with Vario EL III CHN elemental analyzer by using sample weights of 2–8 mg.

2.3. X-ray single crystal diffraction structures

The crystal structures for compounds **2**, **3**, **9** and **16** were determined by single crystal X-ray diffraction. Colorless single crystals were obtained from mixture of dichloromethane and ethyl acetate or from slow evaporation of dichloromethane in dry air atmosphere. Some of the compounds remained as gels or waxes despite of continuous efforts to solidify them.

The crystallographic data were recorded with a Kappa APEX II diffractometer at $-120\text{ }^{\circ}\text{C}$ using graphite monochromatized $\text{Mo K}\alpha$ ($\lambda = 0.71073\text{ \AA}$) radiation. The data were processed with Denzo-SMN v0.95.373 [43,44] and the absorption correction for all compounds was performed using SADABS [45]. The structures were solved by using direct methods (SHELXS-97 [46] or SIR2004 [47] and refined on F^2 by full matrix least squares techniques (SHELXL-97 [48]) by using anisotropic displacement parameters for non-hydrogen atoms. All hydrogen atoms were calculated to their ideal positions as riding atoms by using isotropic displacement parameters. The isotropic displacement parameters were fixed to be 20–50% larger than those of the attached non-hydrogen atom. The programs Diamond [49] and Mercury [50] were used for depicting the crystal structures.

2.4. X-ray powder diffraction analyses

The X-ray powder diffraction data was measured with PANalytical X'Pert PRO diffractometer in Bragg–Brentano geometry using Johansson monochromator (α_1 setup) to produce pure $\text{Cu K}\alpha_1$ radiation (1.5406 \AA ; 40 kV, 30 mA) and step-scan technique in 2θ range of $4\text{--}70^{\circ}$. The data was collected by X'Celerator detector in continuous scanning mode with a step size of 0.0167° and using counting time of 40–100 s per step. Programmable divergence slit (PDS) was used to set irradiated length on sample to 10 mm together with 10 or 15 mm incident beam mask. Soller slits of 0.02° rad were used both on incident and diffracted beam side together with anti-scatter slits (4° and 8.7 mm, respectively). The diffraction data was converted from automatic slit mode (ADS) to a fixed slit mode (FDS) data in Highscore Plus v. 2.2c software package before further analyses by the same program package. Powder samples were prepared either on standard steel plate holders (having 10 or 16 mm radius cavity) or on a silicon-made zero-background holder (petrolatum jelly was used as an adhesive). The simulated powder diffraction patterns were calculated by the program Mercury [50] from the CIF-files of the compounds under investigation.

2.5. Thermal properties

The thermal decomposition paths of compounds **1–21** were obtained with Perkin Elmer Diamond TG/DTA. Measurements were carried out using $45\text{ }\mu\text{l}$ open platinum pans under air atmosphere (135 ml/min) at a temperature range of $25\text{--}900\text{ }^{\circ}\text{C}$. To increase temperature resolution, heating rate was controlled automatically (auto-step mode) by monitoring the weight loss gradient using 25 and $175\text{ }\mu\text{g/min}$ thresholds with 20 s heating/cooling rate update interval to slow down from, or speed up to the nominal heating rate of $10\text{ }^{\circ}\text{C/min}$. In practice, primary decomposition of a sample occurred at isothermal conditions readily after the first initiation of the weight loss over $175\text{ }\mu\text{g/min}$ as the speeding up threshold for the heating rate back to nominal rate was set as low as $25\text{ }\mu\text{g/min}$. The observed isothermal steps were $\sim 20\text{ min}$, at shortest, prolonging to $\sim 90\text{ min}$ on some of the QA salts. By this heating method, more precise decomposition temperatures can be acquired as the onset is less affected by the overshoot, that constant and relatively fast heating rates may cause, due to slow kinetics and low heat conductivities; property of many ionic liquids [51,52]. The temperature calibration of the TG/DTA equipment

was carried out using melting points of five reference materials (In, Sn, Zn, Al, Au) at given heating rate. The weight balance was calibrated by measuring a standard weight at room temperature. The sample weights used in the measurements were about $5\text{--}20\text{ mg}$.

The thermal transitions of the QA salts were examined on a power compensation type Perkin Elmer Pyris 1 DSC. DSC measurements were carried out under nitrogen atmosphere (flow rate 50 ml/min) using $50\text{ }\mu\text{l}$ sealed aluminum pans. The sealing was made by using a $30\text{ }\mu\text{l}$ aluminum pan with pinholes to ascertain good thermal contact between the sample and a pan, and to minimize the free volume inside the pan. The temperature calibration was made by using two standard materials (*n*-decane and In) and the energy calibrations by an indium standard (28.45 J g^{-1}). The samples were heated at the heating rate of $5\text{ }^{\circ}\text{C/min}$ either from -60 or $-50\text{ }^{\circ}\text{C}$ to a temperature close to the decomposition temperature of each compound and then cooled at the heating rate of $5\text{ }^{\circ}\text{C/min}$ back to the starting temperature. The cycle was repeated twice. The sample weights used were about $2\text{--}20\text{ mg}$.

2.6. Solid state NMR

^{13}C CP/MAS NMR spectrum was measured to work out the morphology of compound **2**. The spectrum was measured with Bruker Avance 400 spectrometer equipped with 4 mm standard bore CD/MAS probe-head using 4 mm diameter zirconia rotor and Kel-F caps at ambient temperature. The contact time was 2 ms.

3. Results and discussion

3.1. Characterization in liquid and solid state

According to the ^1H , ^{13}C NMR spectra and mass spectra, all of the synthesized QA salts succeeded with rational yields for our purposes (the optimization of preparing methods were out of scope in this study) and appeared to be pure and free of reaction solvents. In case of compounds **8–21** the absence of the bromide ion was confirmed by mass spectra. However, compounds **3**, **10** and **17** are exceptions containing, according to the NMR-studies traces of triethylamine hydrobromide, a side product from the synthesis. The low melting and waxy tetrafluoroborates are somewhat hygroscopic and in these circumstances the elemental analysis of these compounds is challenging. The bromide and tetrafluoroborate salts were soluble in water, and the hexafluorophosphates were insoluble in water, as expected. All compounds were also soluble in dichloromethane, chloroform and acetone but insoluble in diethyl ether and hexane. The hexafluorophosphates with longer alkyl chains dissolved in acetone but the rest of the compounds were insoluble.

3.2. X-ray single crystal diffraction structure analysis

After a successful crystallization four crystal structures were solved. The crystallographic data of compounds **2**, **3**, **9** and **16** are presented in Table 1 and the selected bond angles and distances in Table 2. The structure determination from the powder diffraction data was also tested for some of the more crystalline salts such as **4** and **18**. However, either unambiguous cell candidates were not found, or in case of found cells the quality of the powder diffraction data was not adequate for successful determination of the powder structure.

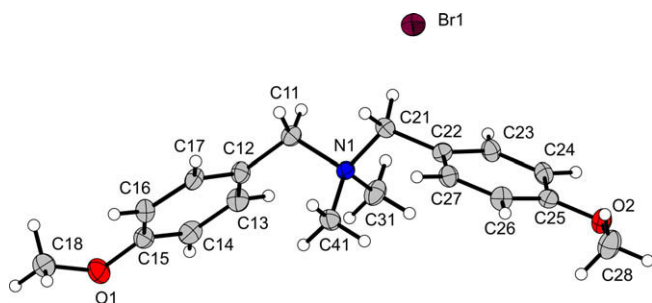
Compound **2** crystallizes in the orthorhombic space group $P2_12_12_1$ having one cation in a slightly distorted *W*-conformation and one Br^- anion in the asymmetric unit as can be seen in Fig. 1. The *W*-conformation resembles the packing of two similar compounds, dimethyldi-(4-methylbenzyl)ammonium bromide

Table 1
Crystallographic data for compounds **2**, **3**, **9** and **16**.

Compound	2	3	9	16
Formula	[C ₁₈ H ₂₄ NO ₂]Br	[C ₁₀ H ₂₄ NO]Br · 1/8 H ₂ O	[C ₁₈ H ₂₄ NO ₂]BF ₄	[C ₁₈ H ₂₄ NO ₂]PF ₆
M _r (g/mol)	366.29	256.46	373.19	431.35
Crystal system	Orthorhombic	Monoclinic	Orthorhombic	Monoclinic
Space group	P2 ₁ 2 ₁ 2 ₁ (No. 19)	P2 ₁ /n (No. 14)	Pna2 ₁ (No. 33)	P2 ₁ /c (No. 14)
a (Å)	8.8971(18)	8.7740(18)	20.527(4)	8.5580(17)
b (Å)	9.3222(19)	9.0660(18)	8.1957(16)	21.159(4)
c (Å)	21.026(4)	33.063(7)	11.164(2)	10.806(2)
β (°)	90	97.18(3)	90	92.66(3)
V (Å ³)	1743.9(6)	2609.4(9)	1878.2(6)	1954.6(6)
Z	4	8	4	4
ρ _{calcd} (g/cm ³)	1.395	1.304	1.320	1.466
μ (mm ⁻¹)	2.364	3.123	0.111	0.210
F(000)	760	1080	784	896
Crystal size (mm ³)	0.1 × 0.5 × 0.1	0.2 × 0.4 × 0.6	0.1 × 0.3 × 0.6	0.2 × 0.2 × 0.2
θ range (degree)	2.39–29	2.34–28.64	2.68–28.85	2.57–29
Reflections collected	27,894	13,294	19,278	31,531
Independent reflections	4496	5390	2506	4990
Data/restraints/parameters	4496/0/203	5390/0/246	2506/1/239	4990/0/257
Goof	1.044	1.021	1.103	1.125
R (int)	0.055	0.0593	0.0819	0.092
Final R indices [I > 2σ(I)]	R ₁ = 0.0327, wR ₂ = 0.0607	R ₁ = 0.0619, wR ₂ = 0.1082	R ₁ = 0.0782, wR ₂ = 0.1271	R ₁ = 0.0890, wR ₂ = 0.2202
R indices (all data)	R ₁ = 0.0479, wR ₂ = 0.0649	R ₁ = 0.1344, wR ₂ = 0.1279	R ₁ = 0.1476, wR ₂ = 0.1461	R ₁ = 0.1324, wR ₂ = 0.2390
Largest diff. peak/hole (e/Å ³)	0.25 and –0.32	0.88 and –0.93	0.25 and –0.31	0.83 and –0.36
Flack parameter	0.065(9)	–	–	–

Table 2
Selected bond lengths (Å) and bond angles (degrees) with e.s.d.s for compounds **2**, **3**, **9** and **16**.

Compound	2	3	9	16
N(1)–C(11)	1.537(5)	1.519(6)	1.503(7)	1.534(5)
N(1)–C(21)	1.530(5)	1.534(6)	1.527(8)	1.528(5)
N(1)–C(31)	1.495(6)	1.522(6)	1.481(8)	1.504(5)
N(1)–C(41)	1.499(6)	1.513(6)	1.503(8)	1.496(5)
C(11)–N(1)–C(21)	106.4(3)	109.0(4)	106.9(5)	109.4(3)
C(11)–N(1)–C(31)	110.1(3)	108.0(4)	110.4(5)	110.4(3)
C(11)–N(1)–C(41)	110.6(3)	111.7(4)	109.8(5)	110.9(3)
C(21)–N(1)–C(31)	109.7(3)	110.3(4)	111.1(5)	106.3(3)
C(21)–N(1)–C(41)	110.2(3)	108.5(4)	110.0(5)	110.7(3)
C(31)–N(1)–C(41)	109.8(4)	109.4(4)	108.7(6)	109.0(3)

**Fig. 1.** The molecular structure and labeling scheme of compound **2**.

and analogous chloride.[53,54] The observed distortion is caused by different orientation of the methoxy group compared to the methyl group at the *para* position of the phenyl group. The packing (Fig. 2a) is affected by Coulombic interactions between the cations and anions, the shortest distance between the nitrogen and bromine atoms being 4.13(1) Å.

Each cation is connected to the Br[–] anion by a weak C–H···Br bond (<3.0 Å), with a bond distance of 2.77(1) Å between H and Br. The same Br[–] anion is connected to a second cation with two C–H···Br[–] bonds, bond distances varying from 2.91(1) to

3.00(1) Å and a third cation with a bond distance of 2.98(1) Å. There is also a weak C–H···Br bond between the anion and an adjacent methyl group, bond length is 2.93(1) Å. The bond angles vary between 135° and 176°. Cations are also packed via intermolecular edge to face π–π interactions between the phenyl groups as can be seen in Fig. 2b.

Compound **3** crystallizes in the monoclinic space group P2₁/n. The ion-pair ordering and the crystal packing are presented in Figs. 3 and 4. The asymmetric unit is composed of two cations and two Br-anions together with one quarter of a water molecule (Fig. 3). The cations pack in a tail-to-tail and head-to-head conformations forming layers along the crystallographic *a*-axis, as can be seen in Fig. 4. The water molecule, along with the second bromine atom in asymmetric unit, is found inside a pocket formed by the cations. Within the pocket there are two possible locations for the water molecule and there are two pockets in the unit cell. The water molecule can be located randomly at each of the four possible positions. Based on a quick search of CSD database [55], compounds with a similar geometrical ordering between bromine and water molecule have also been reported earlier [56]. The packing is further stabilized by weak hydrogen bonds between the cations and anions. Each bromine atom has a C–H···Br[–] (<3.0 Å) bond to four cations, bond distances for Br1 are 2.81(1)–2.88(4) Å and for Br2 2.86(4)–2.98(1) Å. There are also interactions between the water and the Br[–] anion although only the Br2-signed bromine atom in the asymmetric unit forms hydrogen bonds with the water molecule. Each water molecule is connected to two bromine atoms with a bond angle of 129.7° and the distances between the water oxygen and the bromine atoms being 2.79(3) and 3.53(4) Å, respectively. Due to low site occupancy of the oxygen, water-hydrogens could not be found from the electron density map. The shortest distance between the bromine and the nitrogen atom is 4.53(4) Å. The other bromine atom is located inside the layer and has a minimum distance of 4.52(4) Å to the nitrogen atom.

Compound **9** crystallizes in the orthorhombic space group Pna2₁. It differs from the analogous bromide (**2**) by the orientation of the methyls on methoxy groups, which point at the opposite directions. The asymmetric unit is presented in Fig. 5, showing one cation in a slightly distorted W-conformation together with

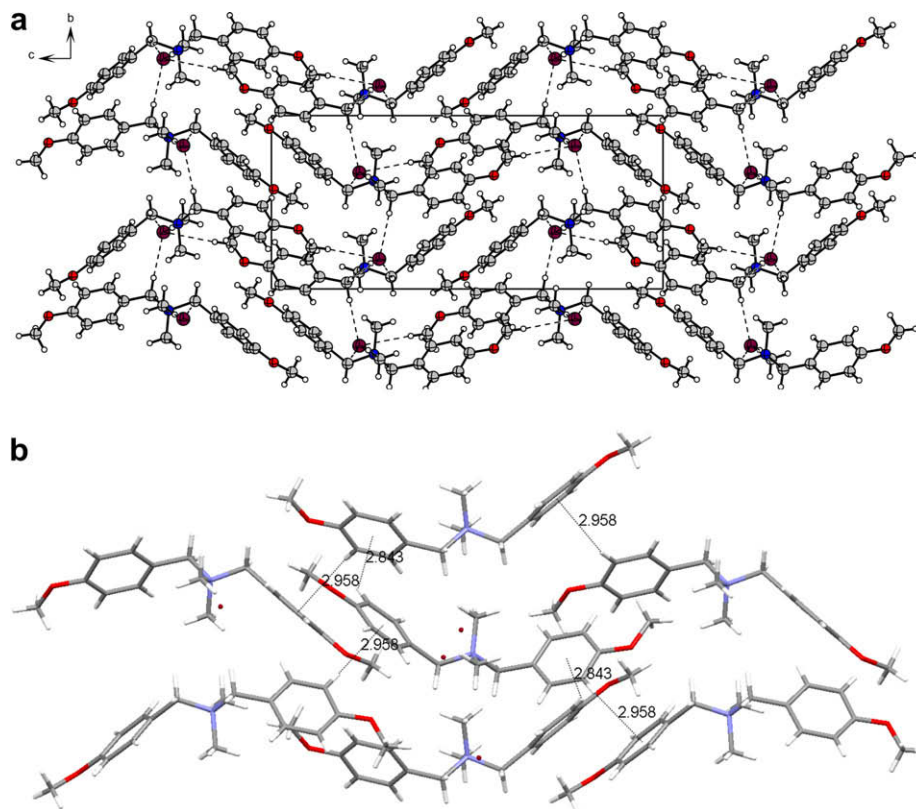


Fig. 2. (a) The packing of compound **2** viewed along the crystallographic *a*-axis. The weak hydrogen bonds are shown as dashed lines. (b) Edge to face π - π interactions forming the network of connections between cations. Some of the cations and anions have been removed for clarity.

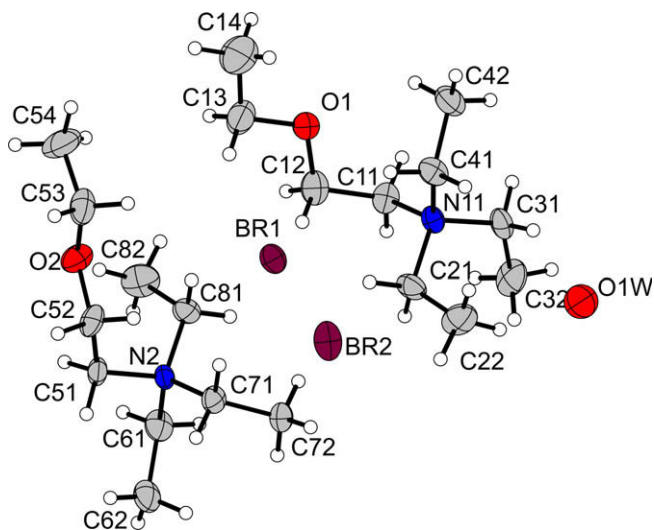


Fig. 3. The molecular structure and labeling scheme of compound **3**.

one BF_4^- anion. The packing (Fig. 6) is affected by Coulombic interactions; the shortest distance between a fluorine atom and the nitrogen atom being $\text{F1} \cdots \text{N1}$ 3.81(1) Å. Each anion also share ten C-H \cdots F hydrogen bonds (<2.65 Å) with six nearest cations. The C-H \cdots F bond distance varies between 2.37(1) and 2.64(1) Å with bond angles from 115° to 162°.

Compound **16** crystallizes in a monoclinic space group $P2_1/c$ deviating also from the analogous bromide salt (**2**). The ion-pair ordering and the crystal packing are presented in Figs. 7 and 8. The asymmetric unit consists of one cation, in which the two phenyl groups are strongly turned towards each other, and one PF_6^-

anion. The packing is stabilized by Coulombic interactions and C-H \cdots F hydrogen bonds (<2.65 Å) can also be observed inside the crystal lattice. The shortest distance between the nitrogen and phosphorous atom is 4.86 Å and between nitrogen and fluorine 3.73 Å. Each anion forms 14 hydrogen bonds, six of which are bifurcated, with the six nearest cations as can be seen in Fig. 9a. The length of the C-H \cdots F bonds varies between 2.43(1) and 2.65(3) Å and bond angles between 131° and 168°. Weak intermolecular edge to face π - π interactions connects the cations to each other causing the formation of chain-like structures along the crystallographic *c*-axis (Fig. 9b). The residual electron density is located close (~ 1 Å) to the phosphorous atom.

3.3. X-ray powder diffraction analysis

The experimental powder diffraction data for compounds **2**, **3** and **16** are presented in Fig. 10 together with the simulated patterns obtained from the single crystal structure parameters. The simulated data were obtained by Mercury [50]. The similarities between the bulk composition and the single crystals are obvious for compounds **3** and **16** as can be seen in Fig. 10. Compound **2** forms two different polymorphs in microcrystalline bulk form, which was also confirmed by the solid state NMR measurements. Based on the powder diffraction data, the first polymorph is consistent with the single crystal data. Considering the fact that the result of the elemental analysis is exact and the NMR spectra are unambiguous, the existence of a second polymorph is confirmed. Additionally, a shoulder in the DSC scan can be observed suggesting that the two polymorphs have melting points very close to each other. However, the structure of the second polymorph remained unknown since the indexing of a second polymorph from a mixture cannot be made unambiguously due to the peak overlap with the dominating peaks of the main component.

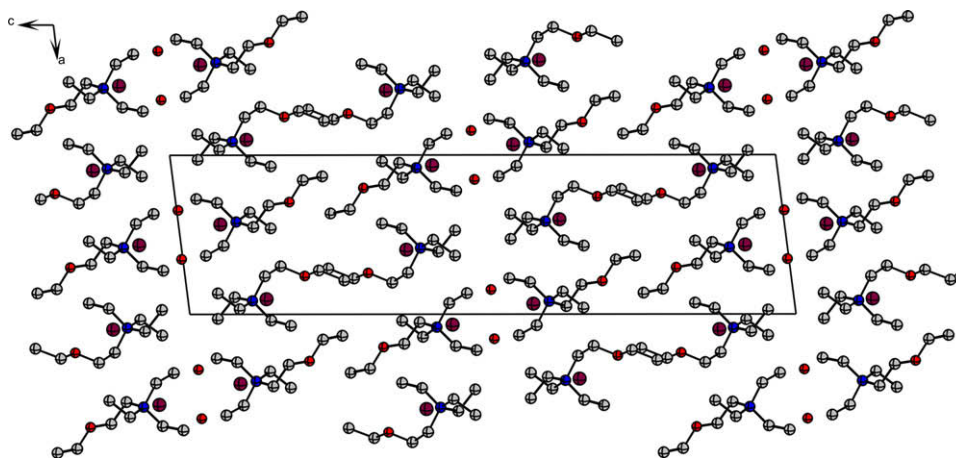


Fig. 4. The packing of compound **3** viewed along the crystallographic *b*-axis. The hydrogens have been removed for clarity.

Compounds **4**, **9** and **12** were crystalline or semi-crystalline (see supplementary material Fig. S1) but did not form single crystals suitable for measurements. For the compounds **16** and **18–21** the crystallinity of the compounds decreases as the alkyl chain length increases (Fig. S2). Due to the platy crystals, especially on compounds **3**, **4**, **12** and **18–21** (microscopy studies revealed the crystals to be nearly two-dimensional and stacked on piles), few diffraction peaks at low 2θ -angle range showed significant preferred orientation, which in part caused the powder structure determinations being unsuccessful. For the semisolids (waxes, gels) powder diffraction measurements were not made.

3.4. Thermal properties

The summarized results of the DSC measurements together with the decomposition temperatures (by TG/DTA) are presented

in Table 3. The results on the second heating scans are also included in the Table 3 to emphasize the tendency for crystallization when compounds are cooled from a liquid state and reheated again. Many of the ionic liquids including some of the salts reported in this study can form glassy states via a supercooled liquid state and thus these compounds can be cooled down without initiation of crystallization [23]. Some of the ionic liquid salts in glassy state can be recrystallized via a cold crystallization when heated above the glass transition temperature, whereas some of the salts will enter to a supercooled liquid state and simply form new glassy state when cooled again below the glass forming temperature.

All the tabulated temperature values from the DSC measurements were taken at peak maximum because rather broad melting

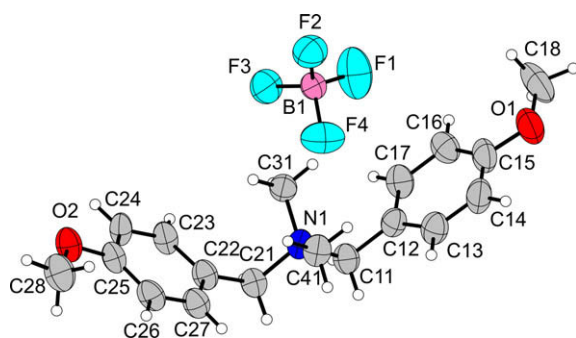


Fig. 5. The molecular structure and labeling scheme of compound **9**.

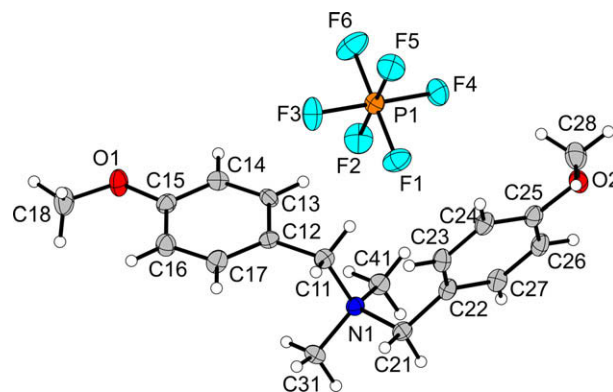


Fig. 7. The molecular structure and labeling scheme of compound **16**.

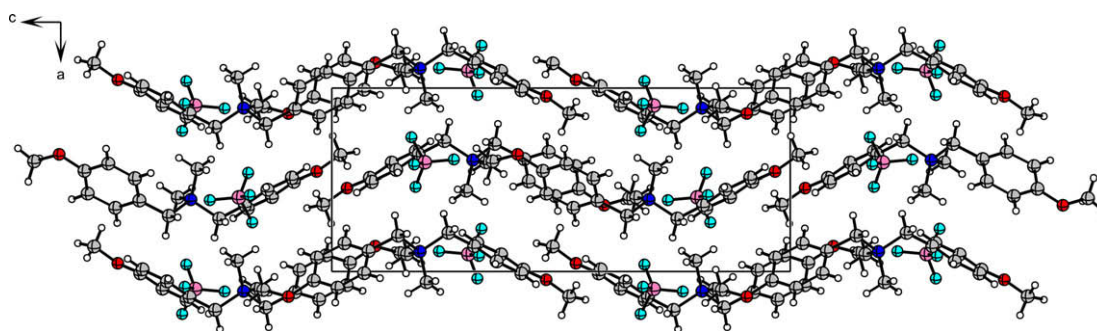


Fig. 6. The packing of compound **9** viewed along the crystallographic *b*-axis.

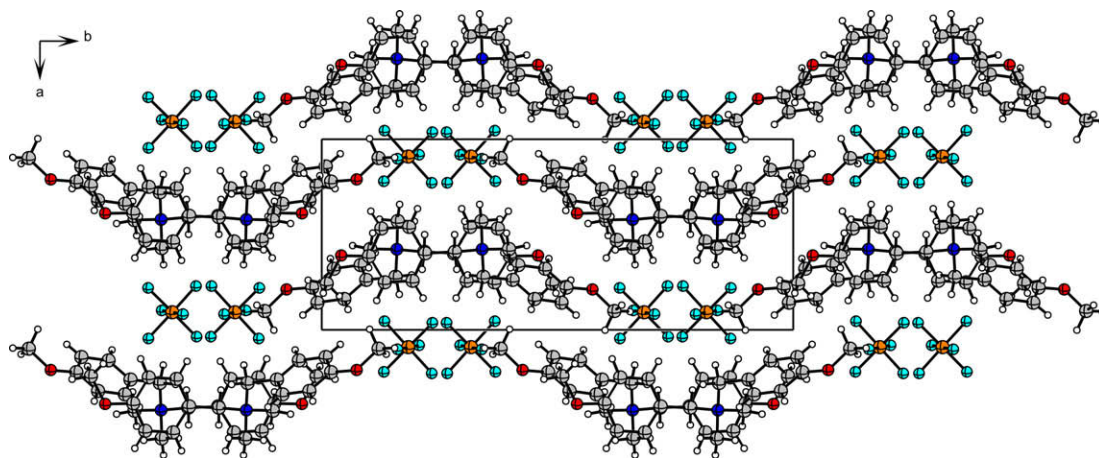


Fig. 8. The packing of compound **16** viewed along the crystallographic *c*-axis.

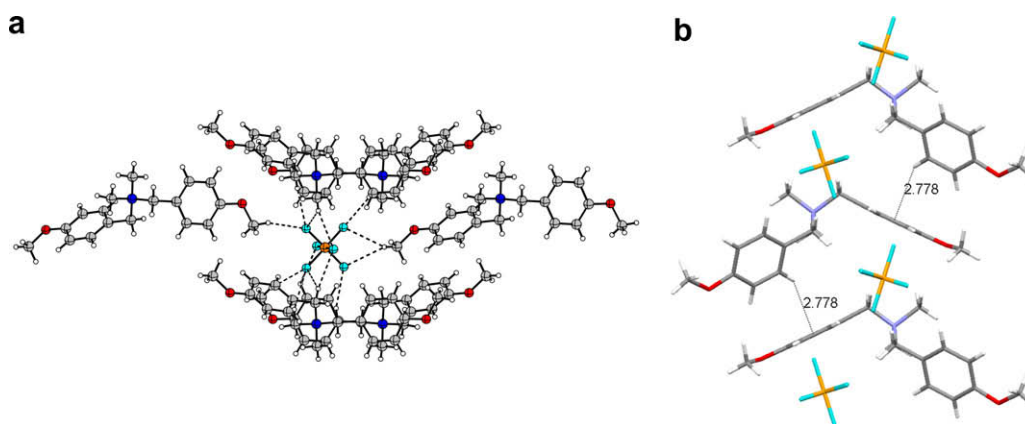


Fig. 9. (a) The weak C–H...F hydrogen bonds (dashed lines) of compound **16**. (b) Edge to face π – π interactions forming the network of connections between cations. Some of the cations and anions have been removed for clarity.

ranges were observed. Typical DSC scans are exemplified in Fig. 11 and the TG curves for compounds **1–21** are presented in Fig. 12. The differences and similarities between the first and the second heating scans (DSC) together with their decomposition onsets are also presented graphically in Fig. 13 (results being arranged both

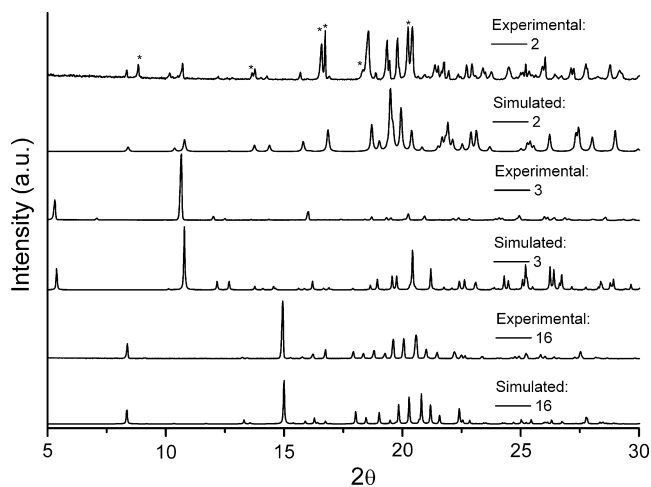


Fig. 10. Experimental powder diffraction patterns of **2**, **3** and **16** compared with simulated data which were obtained from the single crystal structure parameters. Some of the stronger diffraction peaks corresponding to the second polymorph of compound **2** are marked by *.

by similarity of anion and cation) and the liquid ranges together with start and end temperatures are gathered to Table 4.

All the compounds, except **8** and **15**, exhibited a melting transition on first heating scan. Compounds **8** (BF_4^- salt) and **15** (PF_6^- salt) are viscous liquids at room temperature and showed no thermal events on either of the two heating scans. Occasionally a shoulder in the melting transition occurred for compound **2** suggesting that it crystallizes as a mixture of polymorphs, as mentioned earlier. In addition, one of the bromide (**7**) and PF_6^- (**18**) salts exhibited a solid–solid phase transition before melting at -32.4 and 46.5 °C, respectively. These phase transitions were repeatable as transitions were observed also on a second heating. By inspecting the melting temperatures as a function of the anion, it can be noted that the melting points of the bromide salts varied in the range 80 – 176 °C and similarly for BF_4^- salts in the range of 17 – 153 °C. The melting temperatures of BF_4^- salts were typically clearly lower than that of their bromide analogies; the temperature difference between two salt analogies varying ~ 18 – 73 °C. By changing the anion to PF_6^- higher melting temperatures (varying in the range of 25 – 166 °C) were observed when compared to the corresponding BF_4^- salts but still 10 – 30 °C below the melting temperatures of analogous bromides (see Table 4). Compounds **8** and **15** are exceptions to the above-mentioned as they remained as viscous liquids at least till -60 °C, which is the lowest temperature reached by our DSC. In addition, compounds **10** (BF_4^-) and **17** (PF_6^-) exhibited also low melting temperatures, those being ~ 17 and 25 °C, respectively.

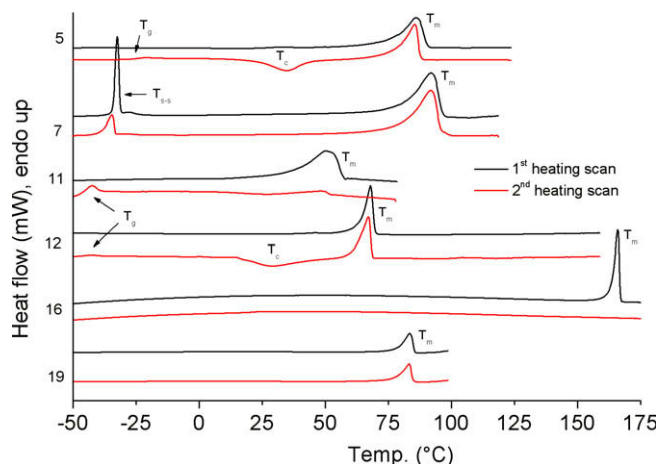


Fig. 11. DSC curves of compounds **5**, **7**, **11**, **12**, **16** and **19** measured under nitrogen with a heating rate of 10 °C/min. T_g , glass transition; T_c , cold crystallization; T_{s-s} , solid–solid phase transition; T_m , melting.

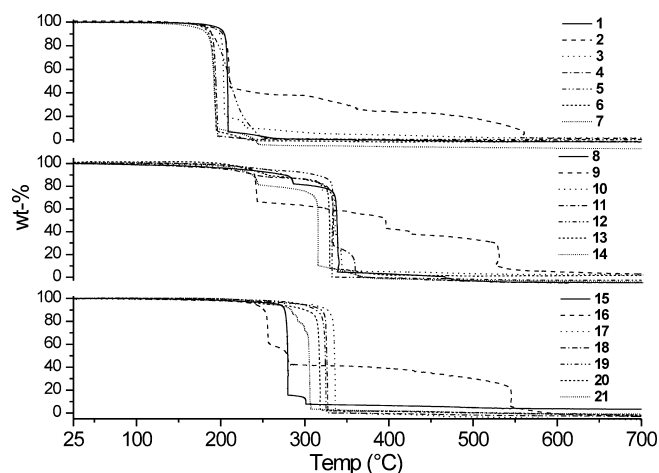


Fig. 12. TG curves of compounds **1–21** measured under air with a heating rate of 10 °C/min.

Further on, the thermal behavior of the prepared QA salts (apart from compounds **8** and **15**) can roughly be divided into three groups based on the observations on the second heating scans. Compounds **3**, **4**, **6**, **7**, **10**, **14** and **17–21** crystallized from a melt while cooled, and re-melted on the second heating similarly as found on first melting (Table 3). Both melting temperatures and their enthalpies observed on the second heating correspond sufficiently to those on the first heating, indicating that the samples have been recrystallized more or less in the same extent. It can be noted, though, that compound **10** was weakly crystalline already from the start as the observed enthalpies were low ($\sim 19 \text{ J g}^{-1}$) on both heating scans. Slightly reduced melting enthalpies were observed also for compounds **4** and **21** on the second heating. The compounds forming the second group (**1**, **5**, **11–13**) supercooled on cooling and turned to a glass as glass transitions were observed at very low temperatures (from ~ -55 to -25 °C). However, on reheating cold crystallization transition was observed above the glass transition which was followed by a remelting at similar temperatures as those found on the first heating scan. Most of the compounds regained the initial extent of crystallinity on cold crystallization but particularly for compound **11** seemingly lesser fraction of the sample recrystallized as the melting enthalpy was

Table 3
Thermal properties for compounds **1–21**.

Compound	1st Heating scan		2nd Heating scan		Decomp. T_d
	T_{s-s} and ΔH	T_m and ΔH	T_g and ΔC_p	T_m and ΔH	
Br⁻					
1	–	79.7 (62.9)	–48.1 [0.33]	80.4 (60.1) ^a	203
2	–	175.5 (69.6)	50.8 [0.42]	–	195
3	–	89.6 (82.2)	–	89.6 (81.1)	193
4	–	102.6 (92.0)	–	92.2 (51.6)	183
5	–	86.0 (55.7)	–25.8 [0.22]	85.5 (46.6) ^a	178
6	–	107.9 (57.6)	–	106.8 (54.7)	184
7	–32.4 (12.8)	92.1 (33.9)	–	91.9 (37.1)	184
BF₄⁻					
8	–	< –60 ^b	–	–	283
9	–	152.6 (67.5)	22.3 [0.32]	–	238
10	–	16.9 (19.0)	–	17.6 (19.9)	267
11	–	50.3 (57.1)	–47.6 [0.32]	48.5 (2.8) ^a	207
12	–	68.1 (72.3)	–46.6 [0.19]	67.1 (65.3) ^a	201
13	–	41.9 (15.5)	–54.3 [0.09]	33.7 (13.8) ^a	199
14	–	45.8 (23.9)	–	55.2 (16.0)	230
PF₆⁻					
15	–	< –60 ^b	–	–	305
16	–	166.0 (82.9)	20.8 [0.33]	–	253
17	–	24.9 (32.6)	–	25.1 (33.9)	315
18	46.5 (9.6)	73.8 (58.6)	–	74.9 (49.6)	320
19	–	83.6 (58.0)	–	83.3 (58.9)	319
20	–	80.6 (33.4)	–	82.0 (29.8)	311
21	–	95.4 (39.4)	–	90.8 (25.0)	293

T_{s-s} , solid–solid transition temperature (°C); T_m , melting temperature; T_g , glass transitions temperature; ΔH , enthalpy of a transition (J g^{-1}); ΔC_p , heat capacity change ($\text{J g}^{-1} \text{ °C}^{-1}$); T_d , decomposition onset by TG/DTA.

^a Exhibits cold crystallization (crystallization on heating) between a glass transition and melting.

^b See text.

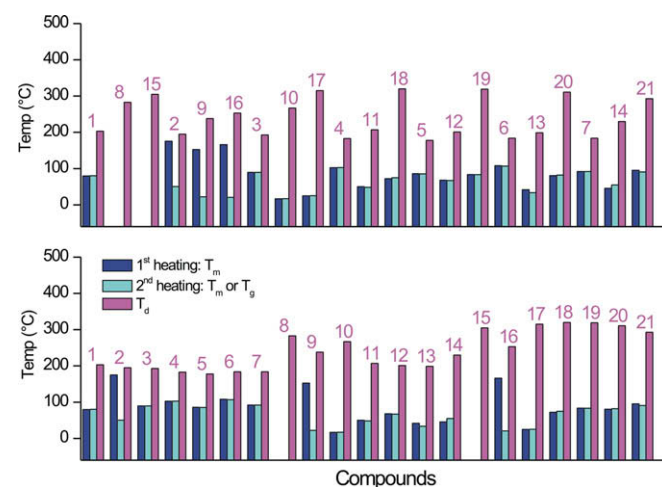


Fig. 13. The T_d and T_m (or T_g) temperatures for compounds **1–21** arranged by same type of the anion (top) and the cation (bottom). In case of the second heating scans, only the melting point is taken account if both glass and melting transitions were observed.

significantly smaller than that found on the first heating (reduced from 57 to 2.8 J g^{-1}). The compounds in the third group (**2**, **9**, **16**; compounds having a dimethyldi-(4-methoxybenzyl)dimethylammonium cation) also showed a tendency to form glassy states by supercooling but instead of cold crystallizing the reheated samples remained as supercooled liquids as only glass transitions were

Table 4
Liquid ranges for compounds 1–21.

Comp.	Bromides (°C)	Comp.	BF ₄ ⁻ salts (°C)	Comp.	PF ₆ ⁻ salts (°C)
1	80–203 (123)	8	–60–283 (343)	15	–60–305 (365)
2	176–195 (19)	9	153–238 (85)	16	160–253 (93)
3	90–193 (103)	10	17–267 (250)	17	25–315 (290)
4	103–183 (80)	11	50–207 (157)	18	73–320 (247)
5	86–178 (92)	12	68–201 (133)	19	84–319 (235)
6	108–184 (76)	13	41–199 (158)	20	81–311 (230)
7	92–184 (92)	14	46–230 (184)	21	96–293 (197)

observed on second heating scans; the bromide having the highest (50.8 °C) and both BF₄⁻ and PF₆⁻ salts having a lower glass transition temperatures at ~22 and 21 °C, respectively.

The decomposition of the bromides occurred mainly in one single stage without identifiable cleavages except for the aralkyl substituted bromide (**2**), as can be seen in Fig. 12. The decomposition started at temperatures 178–203 °C and the compounds decomposed mainly in one stage. Compound **2** decomposed in three stages starting from 195 °C and based on the DSC and TG/DTA measurements the decomposition started during or even before melting. Compared to previously published results for a similar compound, dimethyldi-(4-methylbenzyl)ammonium bromide [53], the decomposition of compound **2** started at a similar temperature, but occurred in several steps. The decomposition of tetrafluoroborates was slightly more complicated than that of the bromides. The decompositions occurred typically in 2–4 steps and compound **9**, analogous to compound **2**, had a decomposition path differing clearly from others (Fig. 12). The decompositions of tetrafluoroborates (**8–14**) started at temperature range 194–283 °C. The decomposition temperatures of all compounds were about 15–80 °C higher than that of the analogous bromides. The thermal decomposition of the hexafluorophosphates (**15–21**) resembled those of the bromides, only the decomposition temperatures were 60–140 °C higher than that of the bromides and 15–120 °C higher than that of the tetrafluoroborates. The decomposition of compound **16** started at 253 °C and for compounds **15** and **17–21** between 293 and 320 °C. Yet again, compound **16** (analogous to compounds **2** and **9**) decomposed having several cleavages, which on the other hand is expected for all three due to their more aromatic nature (phenyl groups). A comparison of these three salts to the structurally similar but non-ether functionalized QA salts (dimethyldi-(4-methylbenzyl)ammonium cation with a same anions) [53,57] reveals that introducing an ether group have only a slight effect on the decomposition temperatures but due to lower melting points, the liquid ranges of the now reported salts are somewhat broader. For the rest of the prepared compounds, comparison of thermal properties to other similar non-ether functionalized salts could not be made as similar compounds either does not exist or they are insufficiently characterized.

Finally it can be concluded that compounds **8**, **10**, **15** and **17** are liquid at room temperature and they are thermally stable remaining liquid over a wide temperature range of 343, 250, 365 and 290 °C, respectively (Table 4). Compounds **1**, **3**, **5**, **7**, **11–14** and **18–21** are liquid below 100 °C and compounds **4**, **6**, **9** and **16** above that. The liquid range for these compounds varies between 76 and 247 °C. For compound **2** only a very narrow liquid range was observed because it decomposed readily after melting at 175 °C.

4. Conclusions

Seven R₂R₂N⁺Br⁻ and R₃R₃N⁺Br⁻ quaternary ammonium bromides were synthesized and used as starting materials in anion exchange reactions thus forming analogous tetrafluoroborates and hexafluorophosphates, total of 21 compounds. The crystal struc-

tures of four compounds (**2**, **3**, **9** and **16**) could be determined after recrystallization by X-ray single crystal diffraction, one of which had two different polymorphs according to the powder diffraction data and solid state NMR spectrum.

Comparing analogous compounds with a same cation, decomposition temperatures increases in the following order: Br⁻ < BF₄⁻ < PF₆⁻. The decomposition temperatures of the hexafluorophosphates were about 20–100 °C higher than that of the tetrafluoroborates and 70–140 °C higher than that of the bromides. Four compounds: **8**, **10**, **15** and **17** are liquid at room temperature and have liquid ranges of 224–365 °C thus enabling their possible use as ionic liquids in the future. Several of the other synthesized compounds are liquid under 100 °C and have a broad liquid range and therefore can also be categorized as ionic liquids. The aromatic compounds **2**, **9** and **16** [all three having dimethyldi-(4-methoxybenzyl)ammonium cation] differed clearly from the other studied compounds. Their decomposition temperatures were significantly lower compared to the aliphatic compounds and the liquid ranges were narrower. When comparing compounds **2**, **9** and **16** to the previously published results of similar but non-ether functionalized compounds, it can be observed that introducing an ether group have only a slight effect on the thermal behavior. For the rest of the prepared QA salts, comparison of thermal properties to other similar non-ether functionalized compounds could not be made since this information is yet not available.

Acknowledgements

We thank Ms. Elina Hautakangas for the elemental analyses, Mr. Reijo Kauppinen for the NMR-measurements and Ms. Mirja Lahtiperä for the ESI-TOF MS-measurements. M.K. gratefully acknowledges the financial support of the Inorganic Materials Chemistry Graduate Program.

Appendix A. Supplementary data

CCDC 678519–678522 contains the supplementary crystallographic data for this paper. These data can be obtained free of charge from The Cambridge Crystallographic Data Centre via www.ccdc.cam.ac.uk/data_request/cif.

Supplementary data associated with this article can be found, in the online version, at doi:10.1016/j.molstruc.2009.01.041.

References

- [1] K.R. Seddon, J. Chem. Technol. Biotechnol. 68 (1997) 351–356.
- [2] T. Welton, Chem. Rev. 99 (1999) 2071–2083.
- [3] J.D. Holbrey, K.R. Seddon, Clean Prod. Process. 1 (1999) 223–236.
- [4] M.J. Earle, K.R. Seddon, Pure Appl. Chem. 72 (2000) 1391–1398.
- [5] R. Sheldon, Chem. Commun. 23 (2001) 2399–2407.
- [6] P. Wasserscheid, T. Welton (Eds.), Ionic Liquids in Synthesis, first ed., Wiley-VCH, Germany, 2003.
- [7] J. Dupont, R.F. de Souza, A.Z. Suarez Paulo, Chem. Rev. 102 (2002) 3667–3692.
- [8] V.I. Parvulescu, C. Hardacre, Chem. Rev. 107 (2007) 2615–2665.
- [9] H. Ohno, Bull. Chem. Soc. Jpn. 79 (2006) 1665–1680.
- [10] T. Sato, G. Masuda, K. Takagi, Electrochim. Acta 49 (2004) 3603–3611.
- [11] K. Yuyama, G. Masuda, H. Yoshida, T. Sato, J. Power Sources 162 (2006) 1401–1408.
- [12] R. Kawano, H. Matsui, C. Matsuyama, A. Sato, M.A.B.H. Susan, N. Tanabe, M. Watanabe, J. Photochem. Photobiol. A 164 (2004) 87–92.
- [13] H. Santa-Nokki, S. Busi, J. Kallioinen, M. Lahtinen, J. Korppi-Tommola, J. Photochem. Photobiol. A 186 (2007) 29–33.
- [14] L. Moens, D.M. Blake, D.L. Rudnicki, M.J. Hale, J. Sol. Energy Eng. 125 (2003) 112–116.
- [15] R.G. Reddy, Z. Zhang, M.F. Arenas, D.M. Blake, High Temp. Mater. Process. 22 (2003) 87–94.
- [16] M.E. Van Valkenburg, R.L. Vaughn, M. Williams, J.S. Wilkes, Thermochim. Acta 425 (2005) 181–188.
- [17] J. Qu, J.J. Truhan, S. Dai, H. Luo, P.J. Blau, Tribol. Lett. 22 (2006) 207–214.
- [18] R.P. Singh, R.D. Verma, D.T. Meshri, J.M. Shreeve, Angew. Chem. Int. Ed. 45 (2006) 3584–3601.
- [19] S.T. Handy, Chem. Eur. J. 9 (2003) 2938–2944.

- [20] G.J. Kemperman, T.A. Roeters, P.W. Hilberink, *Eur. J. Org. Chem.* (2003) 1681–1686.
- [21] L. Ferguson, P. Scovazzo, *Ind. Eng. Chem. Res.* 46 (2007) 1369–1374.
- [22] A. Grosse Boewing, A. Jess, *Chem. Eng. Sci.* 62 (2007) 1760–1769.
- [23] P.S. Kulkarni, L.C. Branco, J.G. Crespo, M.C. Nunes, A. Raymundo, C.A.M. Afonso, *Chem. Eur. J.* 13 (2007) 8478–8488.
- [24] J. Dupont, J. Spencer, *Angew. Chem. Int. Ed.* 43 (2004) 5296–5297.
- [25] C. Samori, A. Pasteris, P. Galletti, E. Tagliavini, *Environ. Toxicol. Chem.* 26 (2007) 2379–2382.
- [26] S. Stolte, J. Arning, U. Bottin-Weber, A. Mueller, W. Pitner, U. Welz-Biermann, B. Jastorff, J. Ranke, *Green Chem.* 9 (2007) 760–767.
- [27] Q. Liu, M.H.A. Janssen, F. van Rantwijk, R.A. Sheldon, *Green Chem.* 7 (2005) 39–42.
- [28] H.S. Schrekker, M.P. Stracke, C.M.L. Schrekker, J. Dupont, *Ind. Eng. Chem. Res.* 46 (2007) 7389–7392.
- [29] N. Menshutkin, *Z. Phys. Chem.* 5 (1890) 589.
- [30] H.Z. Sommer, L.L. Jackson, *J. Org. Chem.* 35 (1970) 1558–1562.
- [31] H.Z. Sommer, H.I. Lipp, L.L. Jackson, *J. Org. Chem.* 36 (1971) 824–828.
- [32] Y. Sasson, *Synthesis of Quaternary Ammonium Salts. Handbook of Phase Transfer Catalysis*, 1997, pp. 111–134.
- [33] J. Ropponen, M. Lahtinen, S. Busi, M. Nissinen, E. Kolehmainen, K. Rissanen, *New J. Chem.* 28 (2004) 1426–1430.
- [34] J. Pernak, J. Feder-Kubis, *Chem. Eur. J.* 11 (2005) 4441–4449.
- [35] D. Das, S. Roy, R.N. Mitra, A. Dasgupta, P.K. Das, *Chem. Eur. J.* 11 (2005) 4881–4889.
- [36] K. Hayamizu, S. Tsuzuki, S. Seki, Y. Ohno, H. Miyashiro, Y. Kobayashi, *J. Phys. Chem. B* 112 (2008) 1189–1197.
- [37] F.B. Abramson, R.B. Barlow, M.G. Mustafa, R.P. Stephenson, *Br. J. Pharmacol.* 37 (1969) 207–233.
- [38] K. Akagi, S. Oae, M. Murakami, *J. Am. Chem. Soc.* 79 (1957) 3118–3120.
- [39] R.B. Barlow, K.A. Scott, R.P. Stephenson, *Br. J. Pharmacol. Chemother.* 21 (1963) 509–522.
- [40] F.M. Walsh, D.N. Crouse, A.M. Ajami, U.S. 76-667685, 1977, 10.
- [41] H. Boehme, G. Lerche, *Justus Liebigs Ann. Chem.* 705 (1967) 154–163.
- [42] J. Albadran, N.H. McMurray, *PCT Int. Appl.*, 99-GB2080, 98-15002, 2000, 20.
- [43] Z. Otwinowski, W. Minor, *Meth. Enzymol.* 276 (1997) 307–326.
- [44] Z. Otwinowski, D. Borek, W. Majewski, W. Minor, *Acta Crystallogr. Sect. A Found. Crystallogr.* A59 (2003) 228–234.
- [45] G.M. Sheldrick, vol. 2, University of Göttingen, Germany, 2001.
- [46] G.M. Sheldrick, *Acta Crystallogr. Sect. A Found. Crystallogr.* A46 (1990) 467–473.
- [47] M.C. Burla, R. Caliandro, M. Camalli, B. Carrozzini, G.L. Cascarano, L. De Caro, C. Giacovazzo, G. Polidori, R. Spagna, *J. Appl. Crystallogr.* 38 (2005) 381–388.
- [48] G.M. Sheldrick, *Acta Crystallogr. Sect. A Found. Crystallogr.* A64 (2008) 112–122.
- [49] K. Brandenburg, *Crystal Impact GbR*, Bonn, Germany, 2005.
- [50] C.F. Macrae, P.R. Edgington, P. McCabe, E. Pidcock, G.P. Shields, R. Taylor, M. Towler, J. van de Streek, *J. Appl. Crystallogr.* 39 (2006) 453–457.
- [51] H. Chen, Y. He, J. Zhu, H. Alias, Y. Ding, P. Nancarrow, C. Hardacre, D. Rooney, C. Tan, *Int. J. Heat Fluid Flow* 29 (2008) 149–155.
- [52] M. Kosmulski, J. Gustafsson, J.B. Rosenholm, *Thermochim. Acta* 412 (2004) 47–53.
- [53] S. Busi, M. Lahtinen, J. Ropponen, J. Valkonen, K. Rissanen, *J. Solid State Chem.* 177 (2004) 3757–3767.
- [54] S. Busi, M. Lahtinen, M. Kärnä, J. Valkonen, E. Kolehmainen, K. Rissanen, *J. Mol. Struct.* 787 (2006) 18–30.
- [55] *Cambridge Structural Database*, v.5.29, 2007.
- [56] D. Berthier, T. Buffeteau, J. Leger, R. Oda, I. Huc, *J. Am. Chem. Soc.* 124 (2002) 13486–13494.
- [57] S. Busi, M. Lahtinen, J. Valkonen, K. Rissanen, *J. Mol. Struct.* 875 (2008) 549–559.